Small-angle, high-contrast exoplanet imaging with the L-band AGPM vector vortex coronagraph now offered at the VLT

Dimitri Mawet[a,b], Olivier Absil[c], Julien Milli[a,d], Christian Delacroix[c], Julien H. Girard[a], Jared O'Neal[a], Pierre Baudoz[e], Anthony Boccaletti[c], Pierre Bourget[a], Valentin Christiaens[c], Pontus Forsberg[f], Frederic Gonté[a], Serge Habraken[a], Charles Hanot[c], Mikael Karlsson[f], Markus Kasper[g], Anne-Marie Lagrange[d], Jean-Louis Lizon[a], Koraljka Muzic[a], Eduardo Peña[a], Richard Olivier[h], Nicolas Slusarenko[a], Lowell E. Tacconi-Garman[g], Jean Surdej[c]

[a]European Southern Observatory, Alonso de Córdova 3107, Vitacura, Casilla 19001, Chile;
[b]Jet Propulsion Laboratory, California Institute of Technology, Pasadena, CA 91109, USA;
[c]Département d'Astrophysique, Géophysique et Océanographie, Université de Liège, 17 Allée du Six Août, B-4000 Liège, Belgium;
[d]Institut de Planétologie et d'Astrophysique de Grenoble (IPAG), University Joseph Fourier, CNRS, BP 53, 38041, Grenoble, France;
[e]LESIA, Observatoire de Paris, 5 pl. J. Janssen, F-92195 Meudon, France ;
[f]Department of Engineering Sciences, Ångström Laboratory, Uppsala University, Box 534, SE-751 21 Uppsala, Sweden ;
[g]European Southern Observatory Headquarters, Karl-Schwarzschild-Str. 2, 85748 Garching bei München, Germany ;
[h]GDTech s.a., LIEGE Science Park, rue des Chasseurs Ardennais, B-4031 Liège, Belgium

ABSTRACT

In November 2012, we installed an L-band annular groove phase mask (AGPM) vector vortex coronagraph (VVC) inside NACO, the adaptive optics camera of ESO's Very Large Telescope. The mask, made out of diamond subwavelength gratings has been commissioned, science qualified, and is now offered to the community. Here we report ground-breaking on-sky performance levels in terms of contrast, inner working angle, and discovery space. This new practical demonstration of the VVC, coming a few years after Palomar's and recent record-breaking lab experiments in the visible (E. Serabyn et al. 2013, these proceedings), shows once again that this new-generation coronagraph has reached a high level of maturity.

Keywords: High contrast imaging, coronagraphy, inner working angle, adaptive optics, observing strategy, post-processing

1. INTRODUCTION

High contrast imaging is an attractive technique to search for exoplanets as it provides straightforward means to characterize them and their host system. Indeed, isolating the signal of exoplanets from the glare of their host star enables us to, e.g., measure and constrain their relative orbital motions with precise astrometry, characterize the planetary atmospheres through spectro-photometry, and understand planet-disk interactions. For these reasons, high contrast imaging constitutes one of the main science drivers of todays ground-based near-infrared adaptive optics instruments, such as NACO at the Very Large Telescope.[1,2] In terms of detection of new objects, the current capabilities of NACO have almost been exhausted, a situation faced by most first-generation adaptive optics imagers and even the Hubble Space Telescope. That is not to say that no new discoveries can still be made, but just that we seem to be nearing a plateau, simply because the current parameter space has been combed through pretty thoroughly (note that early surveys were not optimal and could probably be redone). Only a few objects were discovered, and many non-detections reported and statistically interpreted.[3–5] The field is now

Further author information: send correspondence to dmawet@eso.org

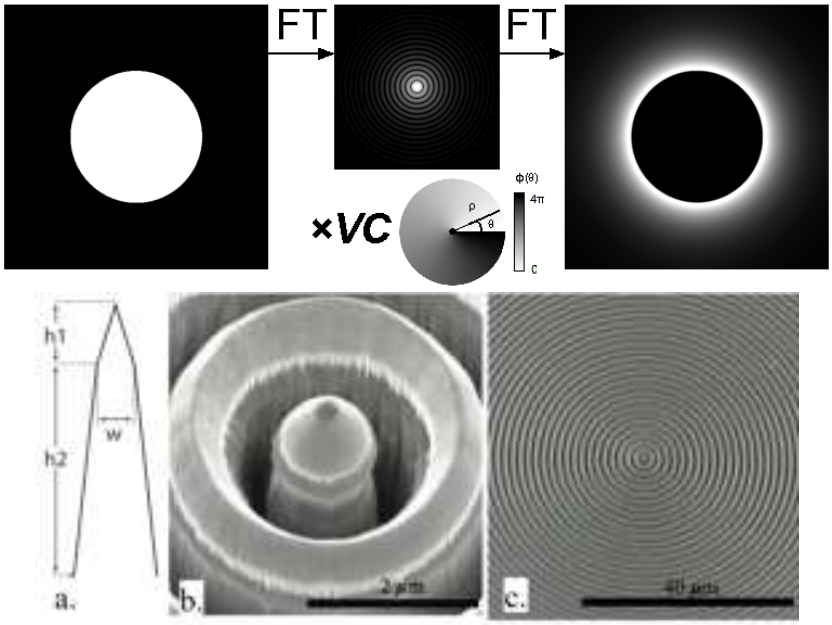

Figure 1. Top: illustration of the diffraction effect of the vortex phase mask on a filled aperture (left). All of the on-axis coherent light appears outside of the geometric image of the input pupil (right). A circular aperture (Lyot stop) then blocks it all. FT stands for Fourier transform.. Bottom: scanning electron microscope (SEM) images of the NACO AGPM. a. Structure profile schematic, with $h_2 = 5 \pm 0.1$ μm, $h_1 = 1 \pm 0.1$ μm, and $w = 0.65 \pm 0.03$ μm (the grating pitch is 1.42 μm). b. Zoom on the center of the diamond AGPM. c. Overview of the structure showing the uniformity and original cleanliness of this particular device.

in need of a technological breakthrough. It is expected that opening the parameter space to fainter/smaller planets closer to their parent stars will indeed bring many new objects.[6] This intermediate parameter space will be opened by the second-generation coronagraphic instruments that have started to arrive at all major observatories: SPHERE at the VLT,[7] the Gemini Planet Imager,[8] P3k-P1640 at Palomar,[9] and ScExAO at Subaru.[10]

These instruments have all been designed around coronagraphs fed by extreme adaptive optics systems, a configuration which is expected to break through the current contrast and inner working angle (IWA) floor. However, first-generation instruments such as NACO still possess untapped potential that only ten years of operations and understanding allow us to fully exploit,[11] especially in the mid-infrared (L' band, from 3.5 to 4.2 μm). This wavelength range offers significant advantages compared to shorter wavelengths:[12] (i) The L-band contrast of planetary-mass companions with respect to their host stars is predicted to be more favorable than in the H band[13–15] so that lower-mass, older objects can be addressed; and (ii) the L-band provides better and more stable image quality, with Strehl ratios well above 70% and sometimes as high as 90%, thus reducing speckle noise. These advantages certainly compensate for the increased sky background in the thermal infrared and the loss in resolution, especially if small IWA phase-mask coronagraphs are available.

2. AN AGPM VECTOR VORTEX CORONAGRAPH ON NACO

The AGPM is an optical vortex made from diamond subwavelength gratings (Fig. 1). When centered on the diffraction pattern of a star seen by a telescope, optical vortices affect the subsequent propagation to the downstream Lyot stop by redirecting the on-axis starlight outside the pupil.[16] The advantages of the AGPM coronagraph over classical Lyot coronagraphs or phase/amplitude apodizers are small IWA, down to $0.9\lambda/D$ (e.g., 0."09 in the L' band at the VLT, slightly smaller than the diffraction limit); clear 360° off-axis field of view/discovery space; outer working angle set only by the instrument and/or mechanical/optical constraints; achromatic over the entire working waveband (here L' band); high throughput (here $\simeq 88\%$); and optical/operational simplicity.

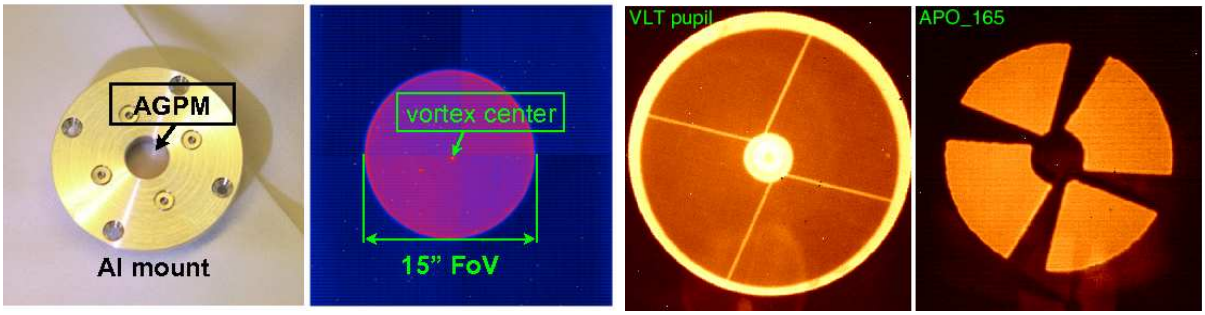

Figure 2. Left: cryogenic Al mount designed by GDTech s.a and view from inside CONICA, showing the 9 mm clear aperture corresponding to a 15" field of view (diameter), fully contained within the 27" field of view of the L27 objective. Middle: full oversized stop of CONICA, showing the VLT pupil (including the central obscuration and struts). Right: APO165 pupil mask (diameter= $0.87 \times D_{pup}$) available inside CONICA, aligned to cover the diffraction and thermal background from the central obscuration and struts.

After eight years of intense technological development, the AGPM has reached a sufficient readiness level for telescope implementation.[17,18] The AGPM selected for NACO was the third one in a series of four realizations (AGPM-L3). Its theoretical raw null depth limited by its intrinsic chromatism was estimated (assuming a trapezoidal profile,* see Fig. 1) and measured to be around 5×10^{-3} (corresponding to a raw contrast of 2.5×10^{-5} at $2\lambda/D$), which is more than needed for on-sky operations where the limit is set by the residual wavefront aberrations.

The AGPM was installed inside NACO as part of a planned overhaul in November 2012. The AGPM was mounted on the entrance slit wheel by means of a dedicated aluminum mount, designed by GDTech s.a. (see Fig. 2, left). The assembly of the mount and AGPM was done on site at Paranal observatory in a clean room environment. Prior to on-sky tests and operations, a CONICA internal image of the mask was done (see Fig. 2), revealing significant dust contamination, marginally affecting the background noise. The slit wheel was set so that the center of the AGPM falls close to but slightly away from CONICA's detector quadrant intersection. The AGPM field of view is $\simeq 15$", corresponding to an outer working angle (OWA) of 7."5. The OWA is only limited by the size of the device (10 mm in diameter) and its mount. The mask transmittance at L' band was measured on the sky to be $85\% \pm 5\%$, which is consistent with the theoretical value and laboratory measurements, both $\simeq 88\%$, limited by imperfect antireflective treatments and mild absorption features around 4 μm.[17] To stabilize speckles, we used the pupil tracking mode enabling angular differential imaging,[20] which is perfectly adapted to the circular symmetry and 360° field of view of the AGPM. The CONICA camera is equipped with a pupil mask which blocks the telescope central obscuration and spiders. Once correctly aligned with the pupil (in x, y, and θ), this mask is optimal for use with the AGPM in pupil tracking mode (see Fig. 2). The measured throughput of the APO165 mask used here is $\simeq 60\%$. In terms of sensitivity, it is worth noting that the throughput loss is almost entirely compensated by the improved thermal background. The pupil obscuration is responsible for more than 25% of the thermal emissivity of the telescope, even though its area only covers $\simeq 5\%$. Therefore, instead of loosing $1 - \sqrt{0.6} \approx 0.225$ in sensitivity, only $1 - 0.6/\sqrt{0.6 * 0.75} \approx 0.1$ is actually lost. To maintain its high contrast capabilities, the centering of the star on the AGPM must be within $(\lambda/D)/10$, or $\simeq 10$ mas (a third of a pixel at L27). This level of centering capability is now routinely obtained with NACO, both in pupil and field tracking modes; we typically measure $\simeq 1$ mas/minute drifts across the meridian.

3. FIRST LIGHT

On December 9, 2012, a representative observing sequence was performed on the 1.9-Gyr old main sequence standard star HD4691 (see Table 1), under $\simeq 1$."2 visual seeing conditions. This star was chosen to maximize brightness and field rotation during the short time allocated for this technical test. A $\simeq 30$-minute ADI sequence

*This AGPM differs from the one tested in Ref. 17. The tops of the grating walls are triangular to improve the transmittance (Fig. 1). This profile was etched with a process similar to the fabrication of broadband antireflective structures.[19]

Table 1. Observing log.

Date	09/12/2012	11/02/2013
Star	HD4691	HD123888
Spectral type	F0V	K1III
V mag	6.79	6.62
L app. mag	5.86	4.01
DIT/NDIT/# fr	0.2s/10/100	0.25s/80/40
Seeing	1" − 1."5	0."8 − 0."9
τ_0	2 − 4ms	4 − 5ms
Strehl ratio	65 − 80%	75 − 80%
PA range	$\simeq 30°$	$\simeq 30°$

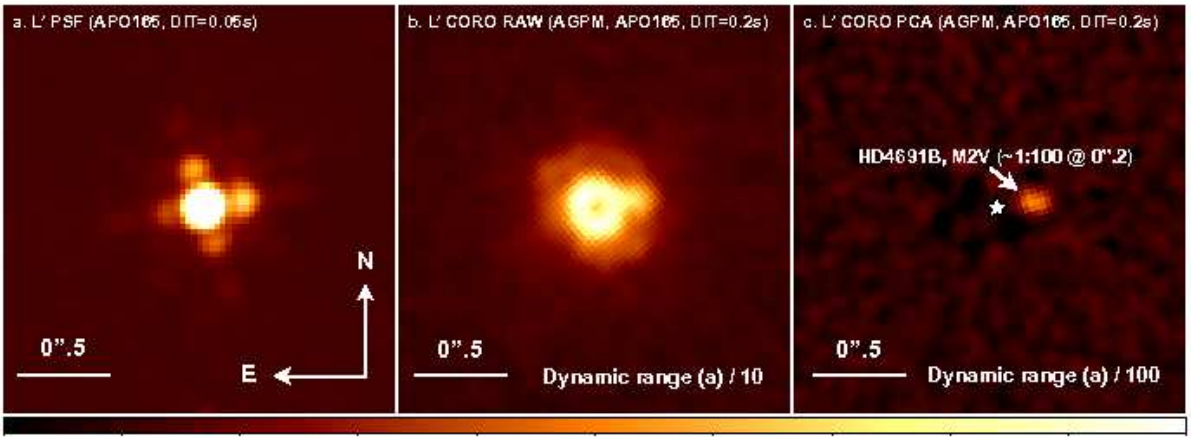

Figure 3. a: L'-band NACO PSF with the APO165 pupil mask in the beam. b: L'-band NACO coronagraphic image with the star centered on the AGPM (the dynamic range and corresponding colorbar/scale are a factor of 10 smaller than in image a). c: Result of our PCA-ADI data reduction pipeline, revealing a putative faint off-axis M2V companion at only $\simeq$ 0."19 (the dynamic range and corresponding colorbar/scale are a factor of 100 smaller than in image a). The scale is linear on all images (and scaled down by a factor of 10 and 100 for b and c, respectively), illustrating in sequence the benefits of coronagraphy and optimized data reduction technique. The bottom color bar refers to Figure a.

was obtained with a parallactic angle (PA) range of 30° and for a total exposure time of 200s on source; the efficiency was mediocre for technical reasons. After acquiring an off-axis PSF for photometric reference, we measured an instantaneous contrast of $\simeq$ 50 peak-to-peak (despite the average-to-bad conditions, see Table 1). The attenuation is about 5 times higher than measured with NACO's four-quadrant phase-mask coronagraph at Ks.[21–23] The coronagraph diffraction control yields two instantaneous benefits compared to classical imaging: (i) the peak saturation limit is decreased by a factor $\simeq$ 50, and (ii) the level of quasi-static speckles pinned to the PSF and the stellar photon noise limit are potentially decreased by a factor $\simeq \sqrt{50} \approx 7$, both within the AO control radius of $7\lambda/D$. All in all, the L'-band AGPM coronagraph allows the background limit to be reached much closer in.

3.1 Detection of a candidate companion

After applying basic cosmetic treatment to our sequence of 100 frames (background subtraction, flat fielding, and bad pixel/cosmic ray correction), we decided to use the quality and stability of the L'-band PSF provided by NACO to perform a sophisticated speckle subtraction. We used the very efficient principal component analysis (PCA) algorithm presented in Ref. 24. The result, using the whole image and retaining three main components, is presented in Fig. 3. By pure chance, the object has a $\simeq 1:100$ (or $\Delta L' \simeq 5$) off-axis companion located at $\simeq$ 0."19 ($< 2\lambda/D$), making this our first unexpected scientific result. The companion flux and astrometry were

obtained by using the fake negative companion technique.[25] The method proceeds as follows: (i) estimate the (biased) position and flux of the companion from the first reduced image; (ii) use the measured off-axis PSF as a template to remove this first estimate from the cleaned data cube before applying PCA; and (iii) iterate on the position x,y and flux until a well-chosen figure of merit is minimized (χ^2 in a pie chart aperture centered on the first estimate of the companion position, $2.44\lambda/D$ in radius and $6 \times 1.22\lambda/D$ in azimuth). The minimization was performed with the Simplex-Amoeba optimization.

Close to the center where the speckle field is intense, the companion flux can be overestimated because the minimization tries to subtract underlying speckles. To estimate our error bars, we decided to proceed with an alternative method called smart-ADI PCA: the frames used to construct the component basis are selected according to a minimum azimuthal separation criterion (here $N_\delta = 0.7\lambda/D$). With this technique, flux is much better preserved. We measured up to 200% additional flux compared to normal ADI PCA. However, fake planet tests still indicate a 25% flux loss, confirming that this method underestimates the flux and thus provides our lower bound. Finally, the coronagraph off-axis attenuation profile, measured in the lab[17] was also taken into account. Using the BCAH98 model,[26] we derived the properties of the newly discovered candidate companion, assuming association. Note that the TRILEGAL starcount model[27] yields a probability of 4×10^{-7} that it is an unrelated background object. At an absolute L'-band magnitude of 6.65, and 1.9 Gyr for the system, the putative companion would most likely be an M2V star at projected separation of 11.8 ± 0.4 AU, and $354.^\circ5 \pm 0.^\circ6$ position angle (see Table 2).

3.2 Representative NACO AGPM detection limits

Since the presence of the companion affects the contrast, we took another similar representative ADI sequence on a different standard star (HD123888, see Table 1). This technical test was performed under better conditions, and benefited from our improved mastering of the new mode (efficiency was four times better than during the first light). A similar instantaneous attenuation was confirmed. To calibrate our detection limits against flux losses induced by PCA, we injected fake companions (at 15σ) prior to PCA and measured their throughput after PCA. We used the derived throughput map to renormalize the initial contrast curve a posteriori (see Fig. 4). Figure 4 shows excellent detection capabilities down to the IWA of the AGPM. The final calibrated contrast presented here (green dash-dot curve), is limited by the small PA range, especially at small angles. The floor reached beyond 1" is due to the background at L', and will be lower for brighter targets and/or longer integrations.

We would like to raise several flags that we will thoroughly address in subsequent papers: (i) Classical tools assuming Gaussian statistics, perfectly valid at large separation, lose significance close to the center simply because the sample size decreases dramatically. At a given angular separation r (in λ/D), there are $2\pi r$ resolution elements, i.e., only 6 at $r = 1\lambda/D$, 12 at $r = 2\lambda/D$, etc. (ii) The probability density function (PDF) of speckle noise and associated confidence level for detection depend on radius. ADI was shown to transform speckles' modified Rician PDF into quasi-Gaussian PDF at large separations, but it is expected that this property of ADI does not hold true at small angles.[28] (iii) The flux attenuation induced by ADI, potentially significant at small angles, does not scale linearly with the companion brightness, which makes its calibration more difficult. These points should be kept in mind when interpreting contrast curves such as those presented in Fig. 4, but also all contrast/detectivity plots that have been presented so far in the literature for very small angles.

4. SCIENCE VERIFICATION ON β PICTORIS

For the science verification run (31 January 2013), we imaged the inner regions of β Pictoris down to the previously unexplored projected radius of 1.75 AU with unprecedented point source sensitivity (Fig. 5, O. Absil et al. 2013, in preparation). The planet was detected at very high SNR (Fig. 5, inset), enabling precise astrometry and photometry. With the fake negative companion technique used in a multi-parametric optimization (Amoeba), we measured the following parameters: $r = 0.448 \pm 0.01$ (first hint that the planet might be past quadrature), PA $= 211^\circ \pm 1^\circ$, and $\Delta L' = 8 \pm 0.3$ mag. The disk was also clearly resolved (see J. Milli et al. 2013, in preparation).

Table 2. Properties of HD4691B.

Distance	62 pc
Age[29]	1.9 Gyr
Companion abs. L' mag	6.65 ± 0.1
Mass	$\simeq 0.3\,M_{\odot}$
Temperature	$\simeq 3450$ K
Sp Type	M2V
Angular sep.	$0.''190 \pm 0.''007$
Proj. angular sep.	11.8 ± 0.4 AU
Position angle	$279° \pm 0.°6$

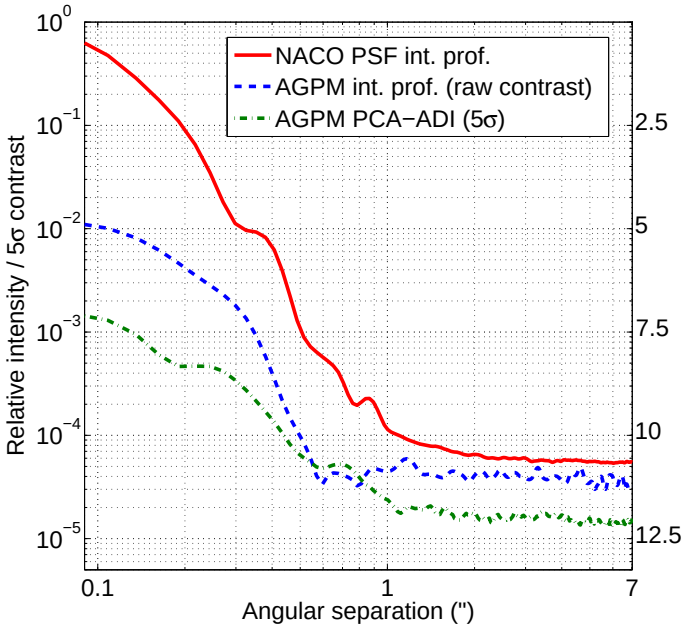

Figure 4. Normalized azimuthally averaged relative intensity profiles and contrast curve. The plain red curve shows the intensity profile of a typical saturated NACO L' PSF (similar brightness and exposure time). The blue dashed curve shows the AGPM intensity profile before PCA, demonstrating the instantaneous contrast gain provided by the coronagraph at all spatial frequencies within the AO control radius ($\simeq 0.''7$). The green dash-dot curve presents the reduced PCA-ADI 5σ detectability limits (40 frames, 800s, $\Delta PA \approx 30°$), taking both the coronagraph off-axis transmission and the PCA-ADI flux losses into account.

5. CONCLUSIONS

The AGPM was designed to provide exquisite IWA (and OWA) capabilities, down to $0.9\lambda/D$ ($0.''09$ at L'), as demonstrated in Fig. 4. The downside of the AGPM's small IWA is its sensitivity to the Strehl ratio (as all coronagraphs) and to pointing errors. The Apodizing Phase Plate (APP) is another advanced coronagraph offered at L'.[30,31] The only, but significant, benefit of this pupil plane phase apodizer over the AGPM is its intrinsic immunity to tip-tilt errors. This advantage, which has to be traded off with the significantly limited field of view provided by the APP, is decisive when tip-tilt is an issue as was the case with NACO prior to November 2011.[11] However, it is less obvious when the instrument provides nominal PSF stability.

In a couple of technical and science verification runs, the L'-band AGPM has proved to be an easy-to-use reliable coronagraphic solution, and one of the best high-contrast imaging modes of NACO (and most likely worldwide). Combined with ADI, we demonstrated that high contrast of the order of $\Delta L' > 7.5$ mag can be

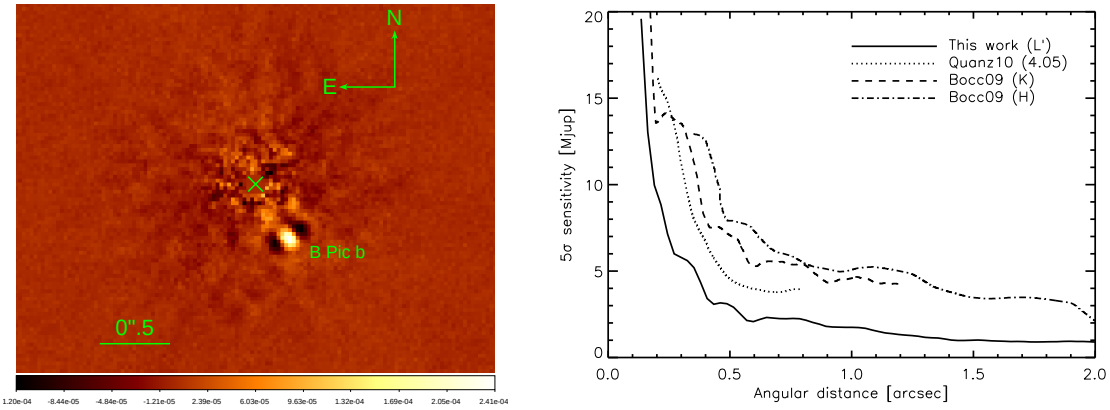

Figure 5. Detection limits in terms of M_{Jup} with the L' NACO AGPM after removing β Picb from the data. We used the BTSETTL model assuming 12 Myr. These detection limits are the best ever presented, despite our conservative "small sample statisctic" corrections to contrast at small angles. We show recent work at shorter wavelengths and with the L band Apodized Phase Plate (APP) for comparison.

reached from the IWA of 0."09 onwards, even with very modest on-source integration time, PA variation, and average conditions. The field of view is a clear 360° discovery space 15" in diameter. The coronagraph is optimized for pupil tracking and is easy to use, thanks to the stability of the NACO L'-band PSF.

ACKNOWLEDGMENTS

This work was carried out at the European Southern Observatory (ESO) site of Vitacura (Santiago, Chile). OA and JS acknowledge support from the Communauté française de Belgique - Actions de recherche concertées - Académie universitaire Wallonie-Europe.

REFERENCES

[1] Lenzen, R., Hartung, M., Brandner, W., Finger, G., Hubin, N. N., Lacombe, F., Lagrange, A.-M., Lehnert, M. D., Moorwood, A. F. M., and Mouillet, D., "NAOS-CONICA first on sky results in a variety of observing modes," in [*Proc. SPIE*], Iye, M. and Moorwood, A. F. M., eds., **4841**, 944–952 (Mar. 2003).

[2] Rousset, G., Lacombe, F., Puget, P., Hubin, N. N., Gendron, E., Fusco, T., Arsenault, R., Charton, J., Feautrier, P., Gigan, P., Kern, P. Y., Lagrange, A.-M., Madec, P.-Y., Mouillet, D., Rabaud, D., Rabou, P., Stadler, E., and Zins, G., "NAOS, the first AO system of the VLT: on-sky performance," in [*Proc. SPIE*], Wizinowich, P. L. and Bonaccini, D., eds., **4839**, 140–149 (Feb. 2003).

[3] Lafrenière, D., Doyon, R., Marois, C., Nadeau, D., Oppenheimer, B. R., Roche, P. F., Rigaut, F., Graham, J. R., Jayawardhana, R., Johnstone, D., Kalas, P. G., Macintosh, B., and Racine, R., "The Gemini Deep Planet Survey," *ApJ* **670**, 1367–1390 (Dec. 2007).

[4] Chauvin, G., Lagrange, A.-M., Bonavita, M., Zuckerman, B., Dumas, C., Bessell, M. S., Beuzit, J.-L., Bonnefoy, M., Desidera, S., Farihi, J., Lowrance, P., Mouillet, D., and Song, I., "Deep imaging survey of young, nearby austral stars . VLT/NACO near-infrared Lyot-coronographic observations," *A&A* **509**, A52 (Jan. 2010).

[5] Vigan, A., Patience, J., Marois, C., Bonavita, M., De Rosa, R. J., Macintosh, B., Song, I., Doyon, R., Zuckerman, B., Lafrenière, D., and Barman, T., "The International Deep Planet Survey. I. The frequency of wide-orbit massive planets around A-stars," *A&A* **544**, A9 (Aug. 2012).

[6] Crepp, J. R. and Johnson, J. A., "Estimates of the Planet Yield from Ground-based High-contrast Imaging Observations as a Function of Stellar Mass," *ApJ* **733**, 126 (June 2011).

[7] Kasper, M., Beuzit, J.-L., Feldt, M., Dohlen, K., Mouillet, D., Puget, P., Wildi, F., Abe, L., Baruffolo, A., Baudoz, P., Bazzon, A., Boccaletti, A., Brast, R., Buey, T., Chesneau, O., Claudi, R., Costille, A., Delboulbé, A., Desidera, S., Dominik, C., Dorn, R., Downing, M., Feautrier, P., Fedrigo, E., Fusco, T.,

Girard, J., Giro, E., Gluck, L., Gonte, F., Gojak, D., Gratton, R., Henning, T., Hubin, N., Lagrange, A.-M., Langlois, M., Mignant, D. L., Lizon, J.-L., Lilley, P., Madec, F., Magnard, Y., Martinez, P., Mawet, D., Mesa, D., Müller-Nilsson, O., Moulin, T., Moutou, C., O'Neal, J., Pavlov, A., Perret, D., Petit, C., Popovic, D., Pragt, J., Rabou, P., Rochat, S., Roelfsema, R., Salasnich, B., Sauvage, J.-F., Schmid, H. M., Schuhler, N., Sevin, A., Siebenmorgen, R., Soenke, C., Stadler, E., Suarez, M., Turatto, M., Udry, S., Vigan, A., and Zins, G., "Gearing up the SPHERE," *The Messenger* **149**, 17–21 (Sept. 2012).

[8] Macintosh, B. A., Anthony, A., Atwood, J., Barriga, N., Bauman, B., Caputa, K., Chilcote, J., Dillon, D., Doyon, R., Dunn, J., Gavel, D. T., Galvez, R., Goodsell, S. J., Graham, J. R., Hartung, M., Isaacs, J., Kerley, D., Konopacky, Q., Labrie, K., Larkin, J. E., Maire, J., Marois, C., Millar-Blanchaer, M., Nunez, A., Oppenheimer, B. R., Palmer, D. W., Pazder, J., Perrin, M., Poyneer, L. A., Quirez, C., Rantakyro, F., Reshtov, V., Saddlemyer, L., Sadakuni, N., Savransky, D., Sivaramakrishnan, A., Smith, M., Soummer, R., Thomas, S., Wallace, J. K., Weiss, J., and Wiktorowicz, S., "The Gemini Planet Imager: integration and status," in [*Proc. SPIE*], **8446** (Sept. 2012).

[9] Oppenheimer, B. R., Beichman, C., Brenner, D., Burruss, R., Cady, E., Crepp, J., Hillenbrand, L., Hinkley, S., Ligon, E. R., Lockhart, T., Parry, I., Pueyo, L., Rice, E., Roberts, L. C., Roberts, J., Shao, M., Sivaramakrishnan, A., Soummer, R., Vasisht, G., Vescelus, F., Wallace, J. K., Zhai, C., and Zimmerman, N., "Project 1640: the world's first ExAO coronagraphic hyperspectral imager for comparative planetary science," in [*Proc. SPIE*], **8447** (July 2012).

[10] Martinache, F., Guyon, O., Clergeon, C., Garrel, V., and Blain, C., "The Subaru coronagraphic extreme AO project: first observations," in [*Proc. SPIE*], **8447** (July 2012).

[11] Girard, J. H. V., O'Neal, J., Mawet, D., Kasper, M., Zins, G., Neichel, B., Kolb, J., Christiaens, V., and Tourneboeuf, M., "Image quality and high contrast improvements on VLT/NACO," in [*Proc. SPIE*], **8447** (July 2012).

[12] Kasper, M., Apai, D., Janson, M., and Brandner, W., "A novel L-band imaging search for giant planets in the Tucana and ? Pictoris moving groups," *A&A* **472**, 321–327 (Sept. 2007).

[13] Baraffe, I., Chabrier, G., Barman, T. S., Allard, F., and Hauschildt, P. H., "Evolutionary models for cool brown dwarfs and extrasolar giant planets. The case of HD 209458," *A&A* **402**, 701–712 (May 2003).

[14] Fortney, J. J., Marley, M. S., Saumon, D., and Lodders, K., "Synthetic Spectra and Colors of Young Giant Planet Atmospheres: Effects of Initial Conditions and Atmospheric Metallicity," *ApJ* **683**, 1104–1116 (Aug. 2008).

[15] Spiegel, D. S. and Burrows, A., "Spectral and Photometric Diagnostics of Giant Planet Formation Scenarios," *ApJ* **745**, 174 (Feb. 2012).

[16] Mawet, D., Riaud, P., Absil, O., and Surdej, J., "Annular Groove Phase Mask Coronagraph," *ApJ* **633**, 1191–1200 (Nov. 2005).

[17] Delacroix, C., Absil, O., Forsberg, P., Mawet, D., Christiaens, V., Karlsson, M., and Boccaletti, A., "Laboratory demonstration of a mid-infrared
AGPM vector vortex coronagraph," *accepted to A&A* (2013).

[18] Forsberg, P. and Karlsson, M., "High aspect ratio optical gratings in diamond," *Diamond & Related Materials* **34**, 19–24 (2013).

[19] Forsberg, P. and Karlsson, M., "Inclined surfaces in diamond: broadband antireflective structures and coupling light through waveguides," *Optics Express* **21**, 2693–2700 (Jan. 2013).

[20] Marois, C., Lafrenière, D., Doyon, R., Macintosh, B., and Nadeau, D., "Angular Differential Imaging: A Powerful High-Contrast Imaging Technique," *ApJ* **641**, 556–564 (Apr. 2006).

[21] Boccaletti, A., Riaud, P., Baudoz, P., Baudrand, J., Rouan, D., Gratadour, D., Lacombe, F., and Lagrange, A.-M., "The Four-Quadrant Phase Mask Coronagraph. IV. First Light at the Very Large Telescope," *PASP* **116**, 1061–1071 (Nov. 2004).

[22] Riaud, P., Mawet, D., Absil, O., Boccaletti, A., Baudoz, P., Herwats, E., and Surdej, J., "Coronagraphic imaging of three weak-line T Tauri stars: evidence of planetary formation around PDS 70," *A&A* **458**, 317–325 (Oct. 2006).

[23] Boccaletti, A., Augereau, J.-C., Lagrange, A.-M., Milli, J., Baudoz, P., Mawet, D., Mouillet, D., Lebreton, J., and Maire, A.-L., "Morphology of the very inclined debris disk around HD 32297," *A&A* **544**, A85 (Aug. 2012).

[24] Soummer, R., Pueyo, L., and Larkin, J., "Detection and Characterization of Exoplanets and Disks Using Projections on Karhunen-Loève Eigenimages," *ApJl* **755**, L28 (Aug. 2012).

[25] Marois, C., Macintosh, B., and Veran, J.-P., "Exoplanet imaging with LOCI processing: photometry and astrometry with the new SOSIE pipeline," *Adaptive Optics Systems II. Edited by Ellerbroek* **7736**, 52 (July 2010).

[26] Baraffe, I., Chabrier, G., Allard, F., and Hauschildt, P. H., "Evolutionary models for solar metallicity low-mass stars: mass-magnitude relationships and color-magnitude diagrams," *A&A* **337**, 403–412 (Sept. 1998).

[27] Girardi, L., Groenewegen, M. A. T., Hatziminaoglou, E., and da Costa, L., "Star counts in the Galaxy. Simulating from very deep to very shallow photometric surveys with the TRILEGAL code," *A&A* **436**, 895–915 (June 2005).

[28] Marois, C., Lafrenière, D., Macintosh, B., and Doyon, R., "Confidence Level and Sensitivity Limits in High-Contrast Imaging," *ApJ* **673**, 647–656 (Jan. 2008).

[29] Holmberg, J., Nordström, B., and Andersen, J., "The Geneva-Copenhagen survey of the solar neighbourhood. III. Improved distances, ages, and kinematics," *A&A* **501**, 941–947 (July 2009).

[30] Quanz, S. P., Meyer, M. R., Kenworthy, M. A., Girard, J. H. V., Kasper, M., Lagrange, A.-M., Apai, D., Boccaletti, A., Bonnefoy, M., Chauvin, G., Hinz, P. M., and Lenzen, R., "First Results from Very Large Telescope NACO Apodizing Phase Plate: 4 μm Images of The Exoplanet β Pictoris b," *ApJl* **722**, L49–L53 (Oct. 2010).

[31] Kenworthy, M. A., Meshkat, T., Quanz, S. P., Girard, J. H., Meyer, M. R., and Kasper, M., "Coronagraphic Observations of Fomalhaut at Solar System Scales," *ApJ* **764**, 7 (Feb. 2013).